Available online at www.sciencedirect.com
ScienceDirect
Aerosol Science 37 (2006) 1809–1825
Journal of Aerosol Science
www.elsevier.com/locate/jaerosci

Investigation of airborne lead concentrations in relation to Asian Dust events and air mass transport pathways

Ki-Hyun Kim[a,*], Chang-Hee Kang[b], Jin-Hong Lee[c], Kum-Chan Choi[d], Yong-Hoon Youn[e], Sung min Hong[f]

[a] *Department of Earth and Environmental Sciences, Sejong University, Seoul, South Korea*
[b] *Department of Chemistry, Cheju National University, Jeju, South Korea*
[c] *Department of Environmental Engineering, Chungnam National University, Daejon, South Korea*
[d] *Department of Environmental Engineering, Donga University, Busan, South Korea*
[e] *Meteorological Research Institute, Seoul, South Korea*
[f] *Polar Environmental Research Division, Korea Polar Research Institute, KORDI, Inchon, South Korea*

Received 17 May 2006; received in revised form 29 August 2006; accepted 29 August 2006

Abstract

In order to explain the influence of Asian Dust (AD) on metal concentration levels in different sized particles, the analysis of Pb in both particulate matters with an aerodynamic diameter less than 2.5 (PM2.5) and 10 μm (PM10) fractions was made consecutively for every spring season during a four-year study period between 2001 and 2004. To explore the impact of AD, a comparative analysis was made to compile Pb measurement data in two different categories: (1) between the AD and non-AD (NAD) periods and (2) between fine and coarse fractions. The results of our analysis indicated that the concentrations of coarse PM fraction increased significantly during the AD period, whereas an increase in the fine PM fraction was of moderate degree. However, when Pb concentrations were concerned, the patterns tended to change quite considerably in both the time-period (AD and NAD) and the particle fractions group. The distribution of atmospheric Pb in the AD period can be explained in two contrasting manners: either preferential enrichment of Pb due to the intrusion of Pb-polluted fine particles or relative depletion of Pb due to the dominance of coarse particles with poor Pb contents. Comparison of the Pb data based on the back trajectory analysis indicates that the effect of AD can be quite selective between pollutant species. If Pb data collected during the entire study period are divided by transport pathways, the patterns derived for each individual route suggest that air masses retained in the local area are more effective to build up Pb concentration levels than those affected by long range transport process.

Keywords: Lead (Pb); PM2.5; PM10; Coarse particle; Fine particle; Asian Dust; Transport pathway

1. Introduction

Due to a rapid increase in population density and the associated energy consumption, the East Asia region is considered to be a major source of various pollutant emissions (Carmichael et al., 1997; Zhang & Arimoto, 1993). In terms of source potential, this region has already become one of the three major regions of pollutant emissions

* Corresponding author. Tel.: +82 2 499 9151; fax: +82 2 499 2354.
E-mail address: khkim@sejong.ac.kr (K.-H. Kim).

0021-8502/$ - see front matter © 2006 Elsevier Ltd. All rights reserved.
doi:10.1016/j.jaerosci.2006.08.009

along with N. America and Europe. Many previous studies, directed towards the investigations of pollutant emissions or their inventory, have concluded that of the Asian countries, China is playing a key role in the emission inventory because of its rapid growth (McKendry et al., 2001; Perry, Cahill, Schnell, & Cahill, 1999). Indeed, one may refer to the RAINS-ASIA database to see the significant regional contribution of China in the global SO_2 emission inventory (e.g., Arndt, Carmichael, Streets, & Bhatti, 1997). It is reported that the magnitude of SO_2 emission from E. Asia amounted to 33.7 Tg in 1990 with China alone contributing 66% (22.2 Tg) of that total. In contrast, Europe and America were seen to release 37 and 24 Tg of SO_2, respectively, for the identical period (Streets, Tsai, Akimoto, & Oka, 2000).

The air pollution patterns of the Korean peninsula, as commonly observed from most urbanized regions, have been accounted for in terms of both internal (local) and external source processes (e.g., an outside source like China). Because large quantities of airborne pollutants are emitted from China, long range transport of airborne pollutants (LRTAP) from China has the potential to affect the air quality of the Korean peninsula (Chun et al., 2001; Chung & Yoon, 1996; Kai et al., 1988; Lin, 2001). In fact, adverse effects of the LRTAP can be seen most apparently during spring, especially with the occurrence of the Asian Dust (AD) events (Kim, Lee, & Jang, 2002; Kim et al., 2003; Kim, Choi, Yun, & Hwang, 2004; Kim & Kim, 2003). As a result, it is considered an essential task to accurately assess the potential impact of AD on the air quality of the receptor areas.

For the purpose of obtaining quantitative information associated with the potential impact of AD on the Korean peninsula, we have been involved in a project investigating the springtime distribution of PM and the associated metallic components since 2001. In this study, to investigate the behavior of metallic components in relation with the AD phenomenon, we specifically focused on the Pb data sets obtained every spring from 2001 to 2004. Pb was selected for this study, because it is one of the most sensitive indicators for diagnosing airborne pollution patterns (Kim, Kim, & Lee, 1997; Mishra, Kim, Kang, & Choi, 2004). Through a detailed analysis of its fractionation between different particles and between AD and non-AD (NAD) periods, we attempted to characterize the factors and processes governing Pb geochemistry under the environmental conditions of the receptor areas.

2. Materials and methods

The experimental site for the present study (37°32′N (latitude) and 127°04′E (longitude)) is located in the NE sector of Seoul, Korea (Fig. 1). The general characteristics of our study site and sampling tactics were introduced in our previous work (Kim et al., 2003) but can be summarized as follows: collection of PM samples was made on top of the Natural Science Building (being remodeled from the fifth to sixth floor in 2003) of Sejong University, which belongs to the Gwang Jin district of Seoul. This site represents a moderately developed urban area. As the site is surrounded by diverse urban facilities including a large-scale public park (E), residential areas (N and W), and a commercial area (S), it is reasonable to suspect that this particular district is influenced by the combined effects of various anthropogenic source types.

Our collection of PM samples for both the AD and NAD periods were made routinely during most weekdays in the spring months between March and May from 2001 to 2004 ($N = 149$). In Table 1, the frequency patterns of AD and NAD events during the entire study period are compared in terms of all-year round, spring season only, and the coverage of the present study. For the simultaneous collection of PM2.5 and PM10 samples, we employed the PM-sampling system developed by URG Inc. (USA). Actual sampling was made over a period of 24 h (starting around 9 AM for each daily measurement) at flow rates of 1 $m^3\,h^{-1}$ (or 16.67 l min^{-1}) using a 0.5 μm pore size Teflon filter (Advantec MFS, Inc., Japan). The analysis of the metallic components bound on both PM fractions was made by adopting the EPA 3051A method. The PM-bound metals were extracted into an acid solution by a CEM microwave digestion system (Model MARS-5) in the following sequence: filter samples were placed in a Teflon container and treated initially with two concentrated acid solutions (9 ml HNO_3 and 3 ml HCl). They were then heated up to 175 °C for a 10 min duration under microwave and remained in the same condition for 5 min; these metal extracted solutions were then separated using a PVDF syringe filter (0.45 μm Whatman) and diluted with deionized water to yield a final volume of 50 ml.

The extractants of the two PM fractions were then analyzed for their metallic components using the ICP-AES system (Thermo Jarrell Ash, Model IRIS-DUO). The analysis of metallic components was made after dividing all the elements into two data groups based on the expected quantity of target analytes in samples such as: (1) the Radial

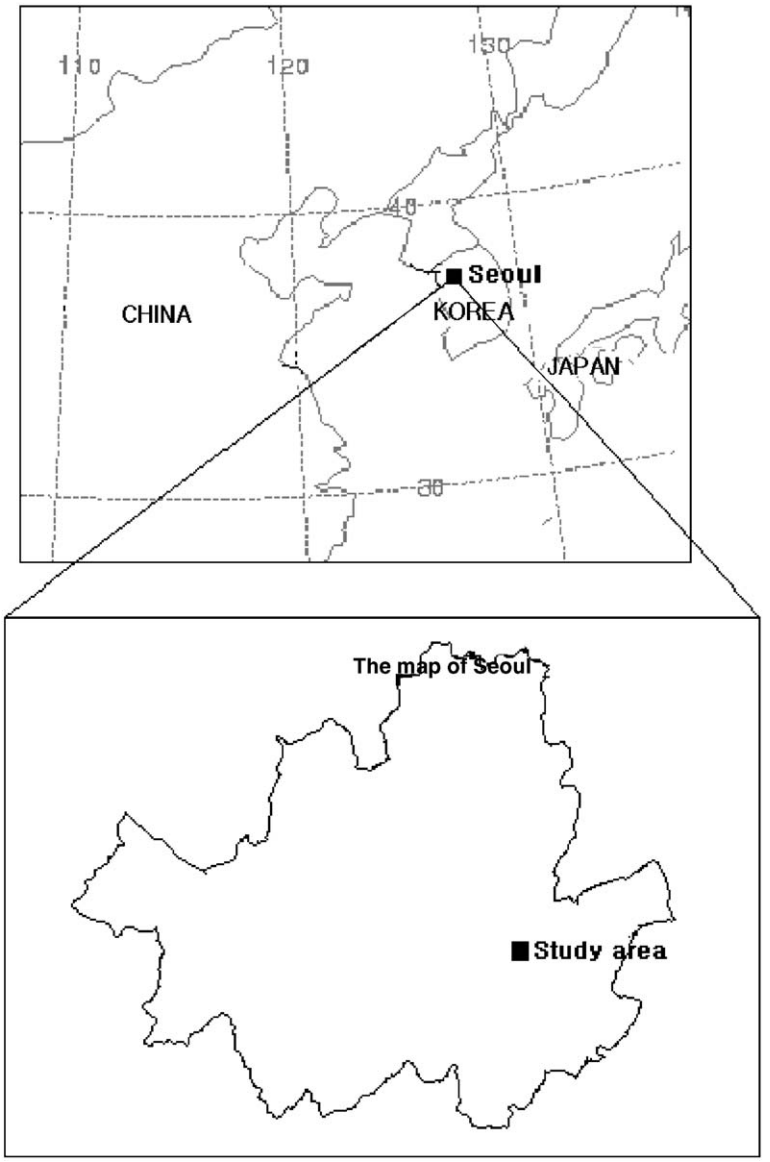

Fig. 1. A geographical location of the study area (Goon Ja Dong in Seoul, Korea) is presented.

Table 1
The occurrence patterns of AD events during the entire study period between 2001 and 2004[a]

	2001	2002	2003	2004
All year	27	15	3	6
Spring season	24	11	3	5
This study	10	10	1	3

[a]The frequency of the AD events are compared between all-year round, spring season only, and the coverage made by this study.

Plasma Torch method for components at high concentration level (Al, Fe, Ca, Na, K, Mg, and S) and (2) the Axial Plasma Torch method for low concentration level (Ti, Mn, Ba, Sr, Zn, V, Cr, Pb, Cu, Ni, Co, Mo, and Cd). Absolute instrumental detection limits for the individual elements investigated in this study can be classified into the following

Table 2
A statistical summary of PM and Pb measurement data obtained during the entire study period[a]

	PM ($\mu g/m^3$)			Pb (ng/m^3)		
	Fine	Coarse	PM10	Fine	Coarse	PM10
	[1] All					
Mean ± SD (Med)	60.3 ± 81.6 (45.5)	55.4 ± 110 (29.1)	98.2 ± 122 (73.8)	86.2 ± 62.5 (68.2)	49.5 ± 44.3 (41.5)	115 ± 74.7 (88.3)
Range (N)	5.90–846 (149)	1.16–1006 (124)	6.21–1073 (147)	20.9–317 (120)	3.17–253 (77)	20.5–347 (123)
	[2] AD					
Mean ± SD (Med)	68.0 ± 42.6 (55.5)	149 ± 215 (87.3)	213 ± 234 (128)	81.5 ± 40.8 (79.1)	39.6 ± 41.9 (26.3)	109 ± 59.5 (114)
Range (N)	25.1–218 (24)	20.3–1006 (23)	78.1–1073 (23)	24.9–183 (21)	3.17–148 (19)	31.8–222 (22)
	[3] NAD					
Mean ± SD (Med)	58.8 ± 87.2 (42.9)	34.1 ± 45.9 (26.1)	76.9 ± 69.3 (65.8)	87.2 ± 66.3 (63.9)	56.9 ± 54.9 (46.3)	111 ± 77.0 (81.0)
Range (N)	5.90–846 (125)	1.16–420 (101)	6.21–587 (124)	20.9–317 (99)	3.60–306 (60)	20.5–347 (109)
A statistical test of differences in the concentration levels between the AD and NAD period						
t	0.504	4.958	5.387	0.378	1.260	0.115
P	0.615	2.33E − 06	2.82E − 07	0.706	0.211	0.909

Comparison is initially made for the whole data set ($N = 149$) between different particle fractions and then extended to both subdivided groups of the AD ($N = 24$) and NAD periods ($N = 125$).

[a]Because of the notation of the coarse fraction (not measured but computed as difference between PM10 and PM2.5), its minimum concentration values are occasionally found to be lower than the analytical detection limits.

three concentration (C) ranges

(1) $10^{-2} \leqslant C < 10^{-1}$ μg: Mn (0.01), Co, Cd, Zn (0.03), Ti, V, and Ni (0.06);
(2) $10^{-1} \leqslant C < 1$ μg: Ba, Cu, Cr, Mo, Sr (< 0.2), Fe (0.4), and Mg/Pb (0.5 ∼ 1.0);
(3) 1 μg $\leqslant C$: Ca (1.0), Na, S (1.5), Al (2.0), and K (3.0).

The absolute detection limit of Pb showed slight variation in the range of 0.5–1.0 μg. Hence, if one considers the total sample volume of around 24 m^3, the minimum detectable concentration of Pb was obtained as low as near 20 $ng\,m^{-3}$ during the laboratory analysis. It should also be noted here that as the concentration of the coarse fraction is obtained as the difference between the PM10 and PM2.5 fractions, negative concentration values were seen occasionally and excluded from the subsequent data analysis. (Refer to Table 2 for the differences in the magnitude of N values between different fractions.) As such, the minimum quantifiable values of the coarse fraction are often found far lower than those of the others.

3. Results and discussion

3.1. The general patterns of PM monitoring between 2001 and 2004

The concentrations of PM-bound metals, including Pb from the PM samples, were measured intensively during every spring period (e.g., months of March, April, and May) between 2001 and 2004. Throughout this four-year period, we were able to measure the concentrations of Pb in each sample from a group of 149 PM samples. To specifically diagnose the impact of the massive springtime dustfall on metal distribution behavior, we divided all measurement data into the AD and NAD periods based on a routine observational report officially made by the Korean Meteorological Research Institute (METRI). According to this classification procedure, 24 of the measurement data fell into the AD class, whilst the other 125 belonged to the NAD class. Hence, the AD/NAD occurrence ratio, if computed using all the data sets, corresponds to a 1:5 relationship. In addition, it is worth examining the annual trend of AD occurrences in our data to explain its temporal variability. Hence, when we allocate those 24 AD data into each respective four-year period (between 2001 and 2004), they correspond to 10, 10, 1, and 3, respectively. The results of this comparison thus show that the occurrence of AD events is dominated by the former two year period (2001 and 2002), covering 83% of the AD events in the four year study period. According to the AD occurrence patterns summarized in Table 1, our study

was made to cover 42, 91, 33, and 60% of the springtime AD events that actually took place during the respective year between 2001 and 2004.

In this study, we intended to evaluate the distribution pattern of atmospheric Pb in terms of its relationship with the AD occurrence pattern. To achieve this, we first computed the concentrations of Pb for different particle fractions, either [1] two classes of PM2.5 and PM10 or [2] three classes of fine (PM2.5), coarse (PM10–PM2.5), and PM10. In Table 2, the concentrations of both PM and the particle-bound Pb are summarized and presented using the above classification criteria. The results, shown in Table 2, indicate that the influence of the AD/NAD relationship is highly distinctive between PM and Pb. If the mean PM concentrations for the NAD period are compared between the two fractions, a notable dominance is apparent for the fine fraction (58.8 $\mu g\,m^{-3}$) relative to coarse one (34.1 $\mu g\,m^{-3}$). However, when the results are compared for the AD data set, the distinction is even clearer with a reversed pattern; the latter with 149 $\mu g\,m^{-3}$ becomes more than two times the concentration of the former with 68.0 $\mu g\,m^{-3}$. Consequently, one may conclude that the occurrences of AD events affect the concentration of coarse particles more effectively than those of fine counterparts. When the differences in absolute concentration values are compared in terms of t-test between the AD and NAD periods, the patterns tend to contrast between the PM and Pb data sets (Table 2). It shows that such differences appear to be significant for both coarse and PM10 data, while it is not the case for all other categories.

If we focus on the results of the Pb measurement data, the patterns are easily distinguishable from those observed in the PM measurement data. Considering that most of the previous Pb measurements tended to focus on its concentration levels in the PM10 (or TSP) fraction, we first compared our PM10 results with those reported from other areas in Korea and Asia. Our present results of PM10-bound Pb concentrations ($115 \pm 74.7\,ng\,m^{-3}$), although measured in a highly urbanized area, appear to be approximately one half of those measured previously from some other urban areas. For instance, the PM10 data from the Daejeon industrial area and a university district in Suwon showed similar results of around 240 $ng\,m^{-3}$ (Kim et al., 1997, 2002). However, our previous study of Pb in various districts of Won Ju revealed that its mean concentrations fell within a wide range between 88 ± 60 (grassland) and $326 \pm 307\,ng\,m^{-3}$ (industrial district) (Kim & Song, 1997). As such, Pb values of a few tens to 100 $ng\,m^{-3}$, which are lower or comparable to the present study, are commonly reported in other areas of the Asia such as the Taichung district, Taiwan (Fang et al., 2002) and Hong Kong (Ho et al., 2003).

Inspection of our Pb data in Table 2 indicates that the dominance of Pb in the fine PM fraction (relative to the coarse fraction) may be a dominant and consistent trend, regardless of period, i.e., whether AD or NAD. From all data sets, Pb in the fine fraction (86.2 $ng\,m^{-3}$) is larger by about 74% than its counterpart in the coarse fraction (49.5 $ng\,m^{-3}$). However, when the periods are separated to allow the examination of the AD influence, the Pb distribution for each fraction changes moderately. As the AD event occurs, reductions in Pb concentrations tend to be apparent from both particle fractions; its concentration in the coarse fraction seems to undergo a considerably significant drop from 56.9 (NAD) to 39.6 $ng\,m^{-3}$ (AD), while that for the fine fraction experiences very little change between the AD and NAD (87.2–81.5 $ng\,m^{-3}$). It can thus be inferred that the occurrences of AD does not noticeably change Pb concentrations in the fine PM mode, whilst alterations in the coarse mode are more noticeable. Hence, the most striking feature of our measurement data can be summarized as follows: although the occurrence of AD events leads to a significant increase in PM mass concentrations in the coarse fraction (i.e., 4.4 times), an opposite trend is confirmed in Pb concentrations in the same particle fraction (i.e., a reduction of two thirds). It is thus most plausible to suspect that most of the incoming particles during the AD period may suffer from Pb depletion by one way or another.

3.2. The analysis of temporal patterns in Pb distributions

In order to analyze the temporal distribution patterns of Pb in our measurement data, we employed a number of approaches. After the initial separation of the AD and NAD data groups, the monthly mean data for the PM and Pb concentrations were computed for both fine and coarse particle fractions. Fig. 2 illustrates the temporal variation patterns of those Pb-associated parameters at monthly intervals for the entire study period. The results of this analysis indicate that PM concentrations maintained notably high levels during the first two years, especially in the second year, while those of the latter two years exhibited a notable decrease. In contrast, the results of the Pb concentration data indicate that their changes are much more complicated across years, as the relative ordering between AD and NAD varies quite significantly across the years.

In Figs. 3 and 4, our results were examined to find the concentration changes in year-to-year and month-to-month intervals, respectively. The year-to-year patterns, shown in Fig. 3, are compared between different particle fractions

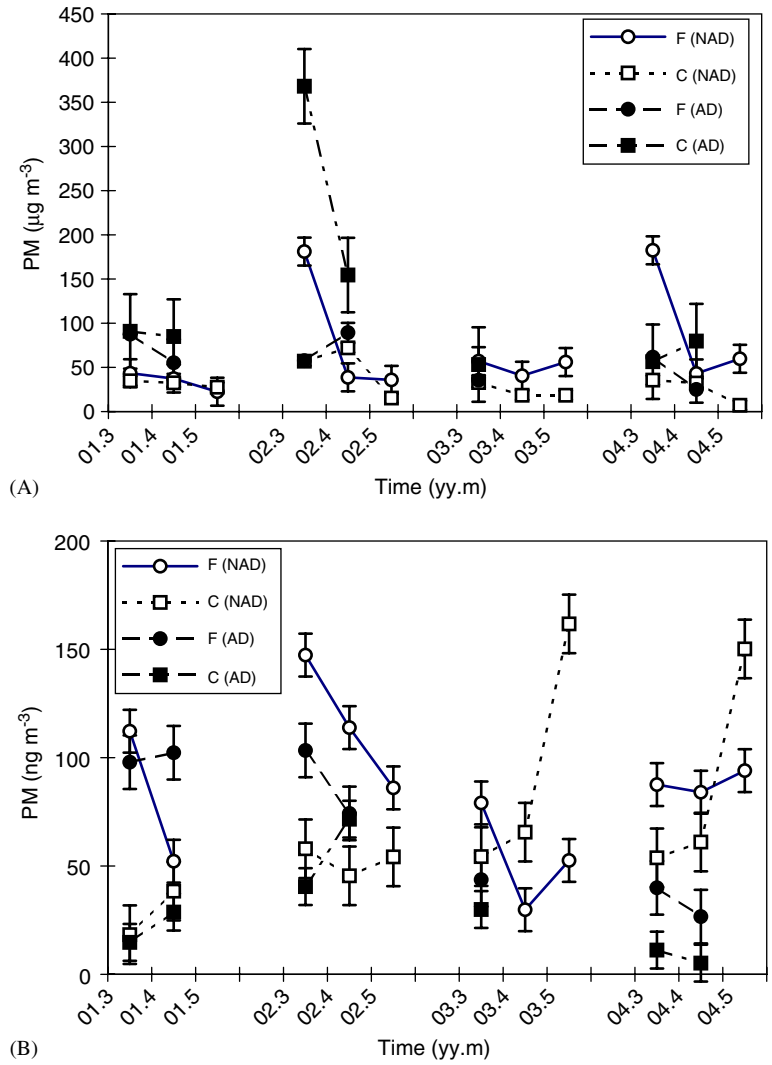

Fig. 2. A plot of temporal variations for PM and Pb using their monthly mean values measured during the entire study period. Errors bars for each monthly data point represent the standard error values.

with (right-hand side) and without distinction of the AD/NAD period (left-hand side). The results with the AD/NAD distinction show the existence of contrasting patterns among different parameters. Especially in the case of PM mass concentration, its increases across the first two years (2001 and 2002) coincide with the frequent occurrences of AD events. However, such a distinction cannot be made in the latter two years, as the PM concentration levels were too small with a lack of data to generalize a trend. It should be noted here that the AD events occurred once in 2003 and three times in 2004.

To evaluate the changes in Pb concentration levels in relation to the influence of AD events, an accurate assessment of the Pb concentration levels in both particle fractions within the time span of the present study is essential. Note that the most prominent patterns of relative Pb distribution are observed from the data sets collected between 2001 and 2002. In the case of the former year (2001), Pb concentrations in the fine mode were much higher by approximately 39% during AD (100 ng m^{-3}) than during the NAD counterpart (72.2 ng m^{-3}). However, an opposite pattern is apparent in the coarse fraction so that the Pb concentration levels contrast between 24.1 (AD) and 32.7 ng m^{-3} (NAD). The results of the year 2002 are however, completely reversed so that relatively enhanced Pb concentrations in the fine and coarse mode are seen from NAD and AD period, respectively. These observations thus support the dual possibility that Pb

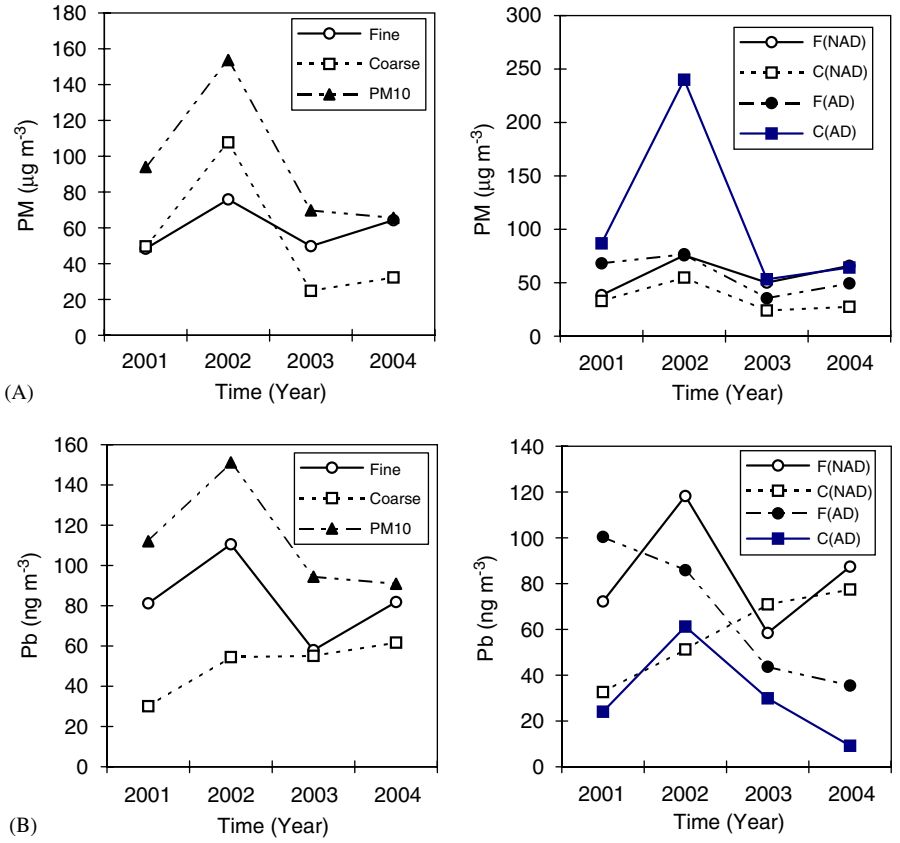

Fig. 3. Temporal changes of PM (top) and Pb (bottom) measured during the entire study period are compared on a year-to-year basis. On the left-hand side, the mean concentrations are compared among fine, coarse, and PM10 fractions. On the right-hand side, comparison is made in a more sophisticated manner with the distinction of the AD and NAD periods for both fine and coarse particle fractions.

concentration levels can be affected by both anthropogenic and natural source processes, if one acknowledges that the metal concentrations are affected by both processes in relation to the particle size range. In addition to our comparison of the patterns across the years, we also attempted to compare the results between different months, regardless of years (in Fig. 4). It should also be noted that AD events were not detected consistently during the month of May for the selected four-year period.

3.3. Factors affecting Pb distributions during the AD events

As summarized in Table 2, Pb concentrations in the fine mode were consistently larger than those in the coarse mode, regardless of data grouping schemes employed. However, if we inspect our data thoroughly, we do note certain differences in the behavior of Pb across the periods. For instance, differences between fine and coarse modes are less significant during AD than during the NAD period. To learn more about the factors governing those differences, it is worth evaluating the Pb data in direct relation with PM concentrations such as Pb/PM concentration ratio.

In Table 3, the relative content of Pb expressed in terms of the Pb/PM ratio is compared both between AD and NAD and between different particle fractions; the ratio is computed as ng m^{-3} divided by μg m^{-3} to yield values multiplied by 10^{-3} (unitless). Inspection of the Pb/PM ratios indicates that AD has a diverse effect on the distribution of Pb for both between the durations and between the particle size fractions. It should be noted that the patterns are quite consistent in the coarse fraction; comparison between AD and NAD across the four-year period indicates that the AD event contributed to lowering its ratios (Fig. 5). Note that its ratio of 2.38×10^{-3} during NAD experiences a three-fold reduction to 0.74×10^{-3} during AD (Table 3).

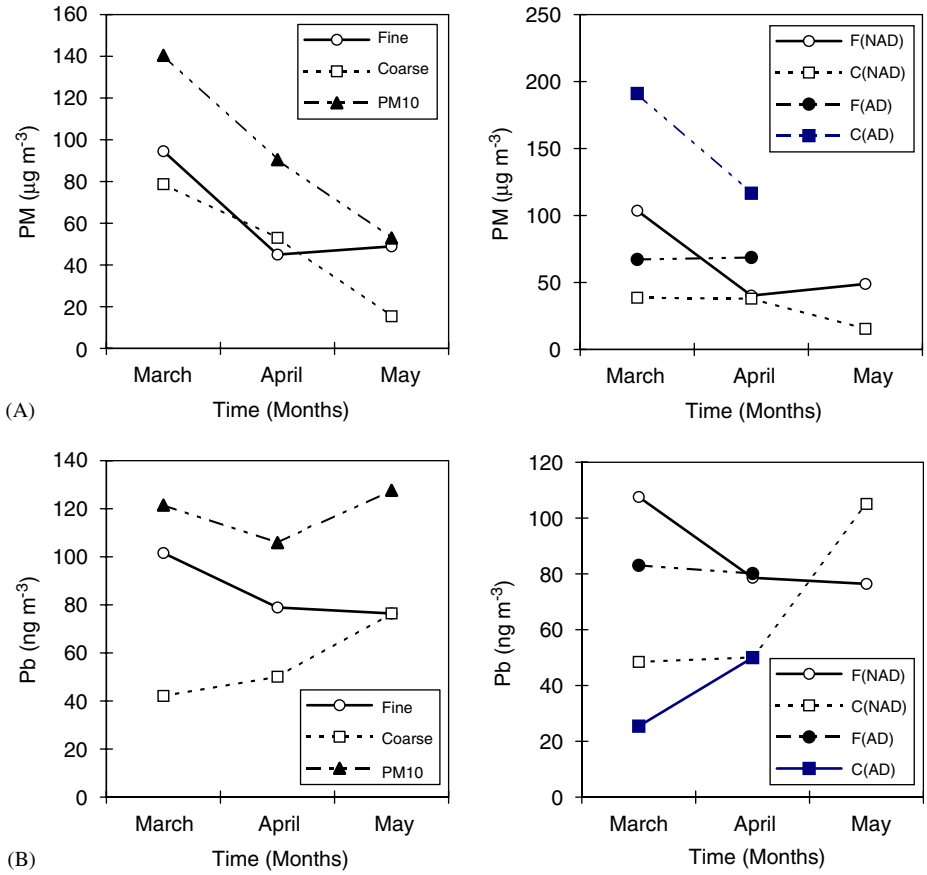

Fig. 4. Temporal changes in the monthly mean concentrations of PM (top) and Pb (bottom) during the entire study period. On the left-hand side, the mean concentrations are compared among fine, coarse, and PM10 fraction. On the right-hand side, comparison is made further between the AD and NAD periods and between fine and coarse particle fractions.

Considering the fact that the total quantity of Pb is dominated by the fine, rather than coarse, fraction, the patterns of Pb/PM ratios in the former fraction have been evaluated in details. As seen in Fig. 5, an inspection of the year-to-year pattern shows that its ratio recorded the most outstanding difference between AD and NAD in 2003. However, we cannot discuss its significance statistically due to the lack of the AD event data for that specific period. Hence, we focused on the results of 2001 and 2002, during which the AD events occurred more frequently than others. These results show that the computed Pb/PM ratios in the fine particle fraction were quite different from the pattern for the coarse fraction; its relative dominance between the AD and NAD periods appears to change quite dramatically between 2001 and 2002.

As another means to examine the factors affecting Pb distribution patterns between the AD and NAD periods, we also conducted a correlation analysis using the Pb data and the relevant parameters with various data grouping schemes (see Table 4). If we compare the correlation results derived for each particle fraction, a number of patterns are apparent. The patterns tend to vary greatly between different particle size fractions and between the AD and NAD periods in terms of correlation strength. It is of interest that the results of the fine fraction contrast sharply between the AD and NAD periods in that the number of strongly correlated cases is abundant during NAD, while it is not the case for AD. More specifically, most metals measured in the fine fraction during NAD (except Cd and Co) showed a probability of no correlations (P) at less than the 0.01 range. On the other hand, the results of the coarse fraction differ between the two periods in that some metals (Si, Ti, V, and Cu) exhibited strong correlations during NAD, while others (Na, S, etc.) during AD. Whilst it is not easy to provide comprehensive explanations for the observed differences in the correlation patterns of the current study, the results of these analyses suggest that local or regional sources are tightly bound to affect the metallic compositions of particles during the NAD period.

Table 3
A statistical summary of concentration ratios derived using PM and Pb measurement data

	Pb/PM[a]			EF(Pb)[b]		
	Fine	Coarse	PM10	Fine	Coarse	PM10
	[1] All					
Mean ± SD (Med)	1.77 ± 1.33 (1.42)	1.73 ± 3.04 (0.96)	1.72 ± 3.35 (1.19)	2075 ± 1908 (1555)	315 ± 658 (150)	678 ± 947 (518)
Range (*N*)	0.06–7.16 (115)	0.03–23.6 (69)	0.04–35.7 (117)	36.6–9777 (120)	5.54–5593 (76)	21.8–9160 (123)
	[2] AD					
Mean ± SD (Med)	1.48 ± 0.91 (1.09)	0.74 ± 1.54 (0.30)	0.80 ± 0.62 (0.61)	417 ± 324 (291)	74.8 ± 99.4 (52.2)	261 ± 588 (104)
Range (*N*)	0.38–4.00 (21)	0.04–6.72 (19)	0.04–2.22 (22)	36.6–1208 (21)	5.54–396 (18)	21.8–2845 (22)
	[3] NAD					
Mean ± SD (Med)	1.82 ± 1.40 (1.50)	2.38 ± 3.71 (1.41)	1.87 ± 3.53 (1.29)	2426 ± 1920 (1855)	668 ± 2096 (271)	788 ± 962 (614)
Range (*N*)	0.06–7.16 (95)	0.03–23.6 (52)	0.28–35.7 (103)	238–9777 (99)	10.7–15578 (60)	86.1–9160 (109)
	PM10/PM2.5 ratio			Fine/coarse ratio		
	PM	Pb	Al	PM	Pb	Al
	[1] All					
Mean ± SD (Med)	2.01 ± 1.97 (1.67)	1.60 ± 1.03 (1.30)	5.08 ± 4.19 (4.11)	2.82 ± 7.04 (1.36)	4.20 ± 7.52 (1.64)	0.64 ± 1.60 (0.30)
Range (*N*)	0.07–17.6 (145)	0.25–6.84 (107)	0.19–36.0 (147)	0.06–61.3 (124)	0.17–43.1 (77)	0.03–16.8 (137)
	[2] AD					
Mean ± SD (Med)	3.31 ± 2.95 (2.50)	1.47 ± 0.62 (1.40)	4.00 ± 1.94 (3.55)	0.82 ± 0.77 (0.67)	6.49 ± 11.1 (2.14)	0.43 ± 0.26 (0.38)
Range (*N*)	1.26–16.2 (23)	0.35–3.00 (21)	0.19–8.66 (23)	0.07–3.92 (23)	0.50–43.1 (19)	0.13–1.11 (22)
	[3] NAD					
Mean ± SD (Med)	1.76 ± 1.62 (1.61)	1.63 ± 1.11 (1.29)	5.28 ± 4.46 (4.16)	3.28 ± 7.72 (1.49)	3.45 ± 5.83 (1.26)	0.68 ± 1.74 (0.30)
Range (*N*)	0.07–17.6 (122)	0.25–6.84 (86)	0.48–36.0 (124)	0.06–61.3 (101)	0.17–37.1 (58)	0.03–16.8 (115)

Comparison is made for the entire data set between different particle fractions and then extended to both subdivided groups of the AD and NAD periods.

[a]The Pb/PM ratio (ng μg^{-1}) should be multiplied by a factor of 10^{-3}.

[b]All EF values are based on Al reference.

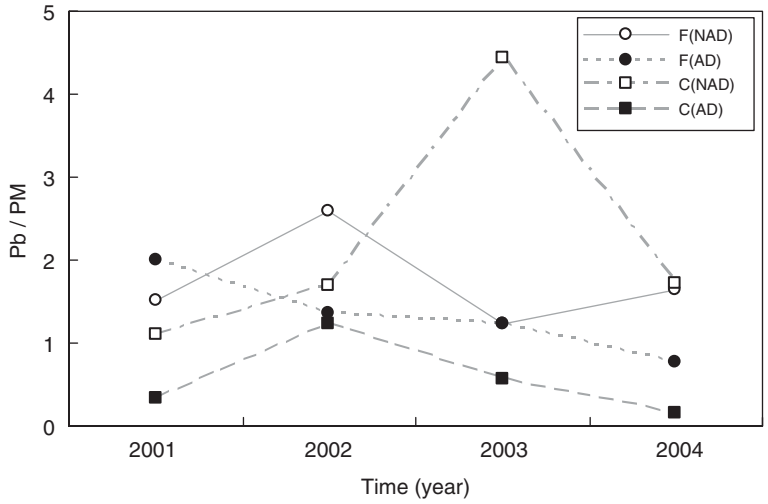

Fig. 5. A plot of annual changes in Pb/PM concentration ratio across the entire study period. These concentration ratios are compared between the AD and NAD periods for both fine and coarse particle fractions. The ratios shown on the *y*-axis should be multiplied by 10^{-3}.

Table 4
The results of correlation analysis between Pb concentrations and the relevant parameters

		Fine fraction			Coarse fraction			PM10 fraction		
		All	AD	NAD	All	AD	NAD	All	AD	NAD
PM	r	0.080	0.205	0.073	−0.147	−0.077	−0.141	0.093	−0.115	0.368[II]
	p	3.96E − 01	3.74E − 01	4.84E − 01	2.27E − 01	7.53E − 01	3.27E − 01	3.21E − 01	6.09E − 01	2.40E − 04
	n	116	21	95	69	19	50	117	22	95
Al	r	0.123	0.260	0.534[II]	−0.098	−0.069	−0.029	0.121	0.057	0.483[II]
	p	1.81E − 01	2.55E − 01	1.21E − 08	3.99E − 01	7.86E − 01	8.28E − 01	1.81E − 01	8.00E − 01	3.12E − 07
	n	120	21	99	76	18	58	123	22	101
Fe	r	0.246[II]	0.227	0.557[II]	0.011	−0.036	0.139	0.203[I]	0.062	0.444[II]
	p	7.11E − 03	3.22E − 01	2.47E − 09	9.25E − 01	8.87E − 01	2.97E − 01	2.46E − 02	7.83E − 01	3.39E − 06
	n	119	21	98	76	18	58	123	22	101
Ca	r	0.198[I]	0.271	0.461[II]	−0.079	−0.231	0.106	0.197[I]	−0.016	0.505[II]
	p	3.04E − 02	2.34E − 01	1.56E − 06	4.99E − 01	3.57E − 01	4.26E − 01	2.92E − 02	9.44E − 01	7.11E − 08
	n	120	21	99	76	18	58	123	22	101
Na	r	0.320[II]	0.217	0.549[II]	0.260[I]	0.739[II]	0.168	0.348[II]	0.384	0.457[II]
	p	6.25E − 04	3.44E − 01	2.02E − 08	2.73E − 02	4.55E − 04	2.24E − 01	8.15E − 05	7.76E − 02	1.60E − 06
	n	111	21	90	72	18	54	123	22	101
K	r	0.592[II]	0.334	0.795[II]	0.137	0.239	0.328[I]	0.321[II]	0.172	0.612[II]
	p	6.33E − 13	1.39E − 01	1.15E − 18	2.35E − 01	3.24E − 01	1.19E − 02	2.89E − 04	4.44E − 01	6.72E − 12
	n	120	21	99	77	19	58	123	22	101
Mg	r	0.164	0.263	0.307[II]	−0.065	−0.056	0.048	0.146	0.041	0.449[II]
	p	7.41E − 02	2.50E − 01	2.02E − 03	5.79E − 01	8.24E − 01	7.21E − 01	1.07E − 01	8.55E − 01	2.47E − 06
	n	120	21	99	76	18	58	123	22	101
S	r	0.726[II]	0.444[I]	0.744[II]	0.622[II]	0.741[II]	0.633[II]	0.542[II]	0.415	0.555[II]
	p	4.60E − 19	4.36E − 02	1.15E − 18	1.83E − 08	1.02E − 03	6.17E − 07	9.03E − 11	5.47E − 02	1.62E − 09
	n	120	21	99	67	16	51	123	22	101
Ti	r	0.174	0.267	0.484[II]	−0.082	−0.086	0.026	0.401[II]	0.062	0.499[II]
	p	5.75E − 02	2.42E − 01	3.97E − 07	4.82E − 01	7.35E − 01	8.44E − 01	4.33E − 06	7.85E − 01	1.13E − 07
	n	120	21	99	76	18	58	123	22	101
Mn	r	0.398[II]	0.238	0.708[II]	0.050	0.007	0.337[II]	0.212[I]	0.118	0.541[II]
	p	7.45E − 06	3.00E − 01	4.90E − 18	6.68E − 01	9.79E − 01	9.65E − 03	1.85E − 02	6.02E − 01	5.02E − 09
	n	119	21	98	76	18	58	123	22	101
Ba	r	0.365[II]	0.355	0.439[II]	0.182	−0.145	0.337[I]	0.304[II]	0.086	0.431[II]
	p	4.57E − 05	1.15E − 01	6.22E − 06	1.17E − 01	5.65E − 01	1.04E − 02	6.53E − 04	7.02E − 01	7.56E − 06
	n	119	21	98	75	18	57	122	22	100
Sr	r	0.133	0.503[I]	0.260[I]	−0.087	−0.061	0.034	0.227[I]	0.050	0.614[II]
	p	1.67E − 01	2.80E − 02	1.33E − 02	5.26E − 01	8.21E − 01	8.39E − 01	1.21E − 02	8.26E − 01	6.87E − 12
	n	109	19	90	55	16	39	122	22	100
Zn	r	0.623[II]	0.700[II]	0.656[II]	0.251[I]	−0.002	0.286[I]	0.407[II]	0.346	0.419[II]
	p	9.13E − 15	4.08E − 04	3.97E − 14	3.87E − 02	9.94E − 01	4.02E − 02	2.98E − 06	1.14E − 01	1.31E − 05
	n	120	21	99	68	16	52	123	22	101
V	r	0.194	0.209	0.604[II]	−0.066	−0.090	0.182	0.209[I]	0.070	0.621[II]
	p	6.22E − 02	3.90E − 01	1.14E − 08	6.36E − 01	7.41E − 01	2.80E − 01	2.08E − 02	7.58E − 01	3.14E − 12
	n	93	19	74	53	16	37	122	22	100
Cr	r	0.228[I]	−0.483[I]	0.279[II]	0.114	0.458	0.089	0.066	0.130	0.058
	p	1.42E − 02	3.61E − 02	5.84E − 03	4.06E − 01	1.34E − 01	5.70E − 01	4.74E − 01	5.64E − 01	5.72E − 01
	n	115	19	96	55	12	43	121	22	99

Table 4 (*Continued*)

		Fine fraction			Coarse fraction			PM10 fraction		
		All	AD	NAD	All	AD	NAD	All	AD	NAD
Pb	r	1.000	1.000	1.000	1.000	1.000	1.000	1.000	1.000	1.000
	p	–	–	–	–	–	–	–	–	–
	n	120	21	99	77	19	58	123	22	101
Cu	r	0.616^{II}	0.460^{I}	0.628^{II}	0.496^{II}	0.315	0.525^{II}	0.587^{II}	0.452^{I}	0.602^{II}
	p	2.57E − 14	3.60E − 02	1.86E − 12	8.28E − 06	2.18E − 01	3.20E − 05	6.27E − 13	3.46E − 02	2.08E − 11
	n	120	21	99	73	17	56	123	22	101
Ni	r	0.200^{I}	-0.448^{I}	0.252^{I}	0.051	−0.013	0.077	0.051	0.060	0.053
	p	3.17E − 02	4.79E − 02	1.39E − 02	6.83E − 01	9.62E − 01	5.99E − 01	5.76E − 01	7.92E − 01	6.01E − 01
	n	115	20	95	66	17	49	123	22	101
Co	r	0.129	0.064	0.142	−0.067	0.062	−0.046	0.177	0.181	0.227^{I}
	p	1.69E − 01	7.93E − 01	1.67E − 01	6.23E − 01	8.32E − 01	7.72E − 01	5.25E − 02	4.21E − 01	2.41E − 02
	n	116	19	97	56	14	42	121	22	99
Mo	r	0.259^{II}	−0.190	0.281^{II}	0.123	0.216	0.062	0.076	0.148	0.065
	p	4.77E − 03	4.10E − 01	5.55E − 03	3.76E − 01	4.22E − 01	7.12E − 01	4.04E − 01	5.12E − 01	5.21E − 01
	n	117	21	96	54	16	38	123	22	101
Cd	r	−0.019	0.425	−0.056	0.263	0.258	0.299	0.412^{II}	0.566^{I}	0.400^{II}
	p	8.50E − 01	1.48E − 01	6.11E − 01	7.37E − 02	4.43E − 01	7.65E − 02	2.52E − 05	3.47E − 02	1.61E − 04
	n	97	13	84	47	11	36	98	14	84

The strengths of correlations are examined for all three particle fractions investigated in this study for all different periods (such as all, AD, and NAD).
Superscripts given in roman letters of I and II denote the significance of correlation at 0.05 and 0.01, respectively (2-tailed).

To a certain degree, the complexity seen in the fine fraction results may reflect the fact that its patterns of long-range transport can be more dynamic due to such factors as enhanced mobility and/or strong affinity for metallic components. Similar to such expectation, Perry et al. (1999) previously suggested the importance of three PM formation/transport process types in LRTAP episodes based on size-segregated measurements of PM mass and composition in Hawaii: (1) anthropogenic aerosols mixed with AD, (2) Asian pollution with small amounts of soil dust, and (3) biomass burning episodes from N. America.

3.4. The relationships between air mass transport route and Pb concentration levels

In the recognition of the significance of LRTAP on metal distributions, we examined the possibility whether and how Pb concentration levels are affected by the AD events with an aid of back trajectory analysis. In some previous studies, it was reported that the type and abundance of the pollutant elements carried by the AD strongly depend on the route of the AS traveled (Sun et al., 2005). In an attempt to describe the effects of air mass transport pathway on trace metal pollution, the movement patterns of air masses were evaluated in relation to back trajectory analysis technique. To this end, the trajectories for comparison were computed for each individual PM measurement made in this study; each trajectory analysis was extended for a 72 h duration to cover up to the midnight of each PM measurement day (00:00 LTC or UTC+9:00). All of this trajectory computation has been made on the basis of diagnostic vertical velocity fields (kinematic) assumption (Draxler, 1996) using the HYSPLIT (Hybrid Single-Particle Lagrangian Integrated Trajectories) model developed by NOAA/ARL (National Oceanic and Atmospheric Administration/Air Resources Laboratory) (Draxler, 2001). As input meteorological data to run the trajectory model, National Centers for Environmental Prediction (NCEP) model output (6-h interval, hemispheric 129 by 129 polar stereographic grids) was also used (Kanamitsu, 1989). The altitude of the starting point for trajectory model calculation was set at 500 m above mean sea level that corresponded to the height within or across the planetary boundary layer.

As seen from the results of back-trajectory analysis, the origin (and/or pathway) of air masses transported to the study site was initially classified into five different categories (Fig. 6): (1) Route 1 (R1—westerly origin): air masses

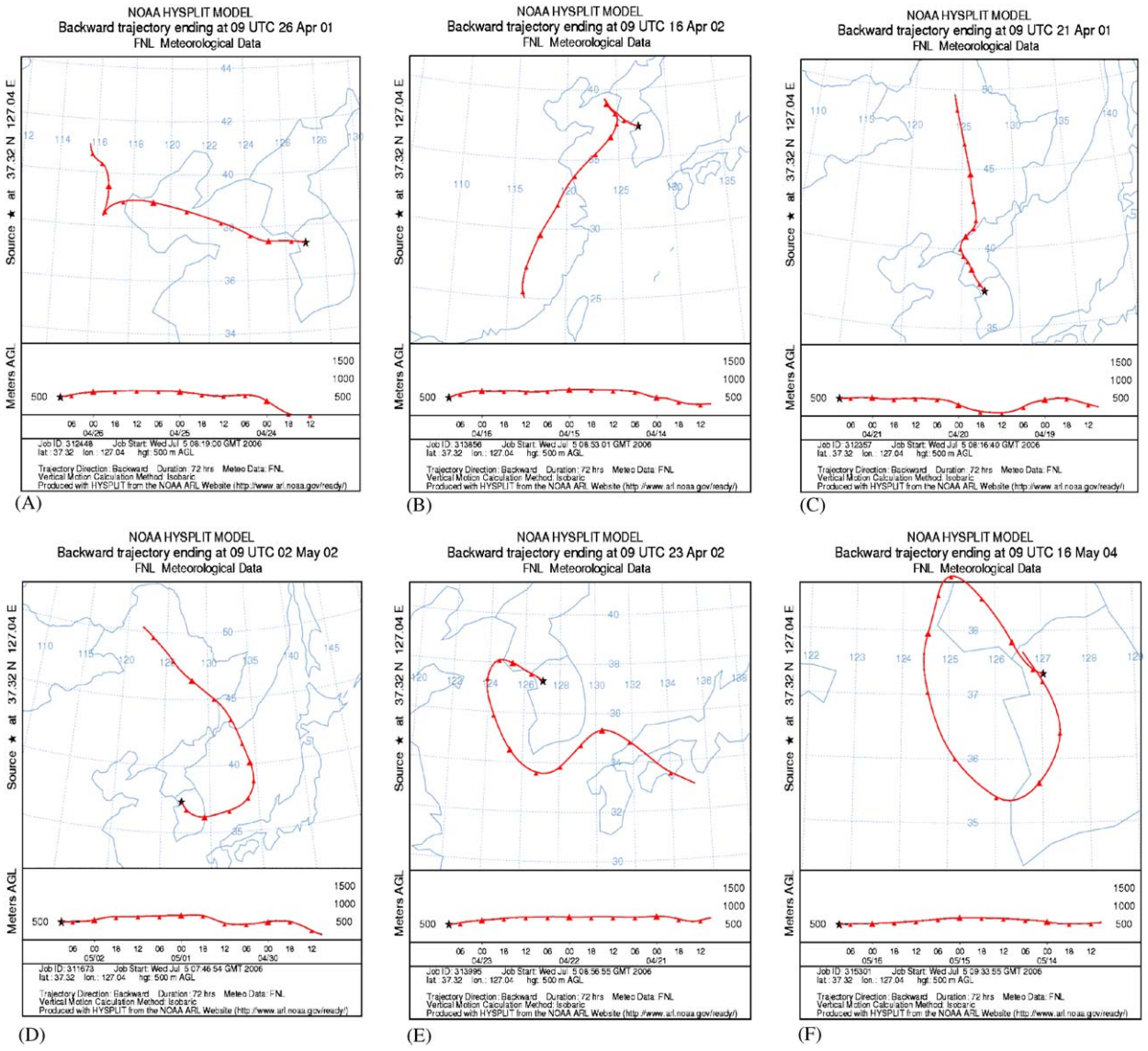

Fig. 6. Air mass movement patterns into the study site (Seoul, Korea) are classified as 6 different route types based on back-trajectory analysis; (A) route type 1A (R1A): passing from N. China; (B) route type 1B (R1B): passing from S. China; (C) route type 2 (R2): passing from N Korea; (D) route type 3 (R3): passing from E. Sea; (E) route type4A (R4): passing from S. Sea; (F) route type 5 (R6): circulating in local area.

coming from China across the Yellow Sea; (2) Route 2 (R2—northerly origin): Russia/N. Korea along the west coast of the Korean peninsula; (3) Route 3 (R3—easterly origin): across the east coast of the Korean peninsula; (4) Route 4 (R4—Southerly): from Japan area or south of Jeju, and (5) Route 5 (R5—no designated direction): locally retained cases. In Fig. 7, the frequency distribution of all transport routes during the entire study period was inspected between AD and NAD period with the entire data sets categorized into the above five route types. Although most results of trajectory analysis are good enough to represent the typical pattern for all five transport routes depicted in Fig. 6, there are also some cases that are by and large altered from such common pathway patterns. Hence, the sum of counting for each trajectory route was distinguished between all (A) and valid (V) cases for all five routes in Fig. 7. According to this notation, valid cases for trajectory analyses, when divided between AD and NAD period, covered 89% and 85% of each data group, respectively.

In light of the occurrence of such distorted transport routes, all numerical computations to derive the representative concentrations for each pathway were made using the data sets with the typical (or non-distorted) cases solely (i.e., the

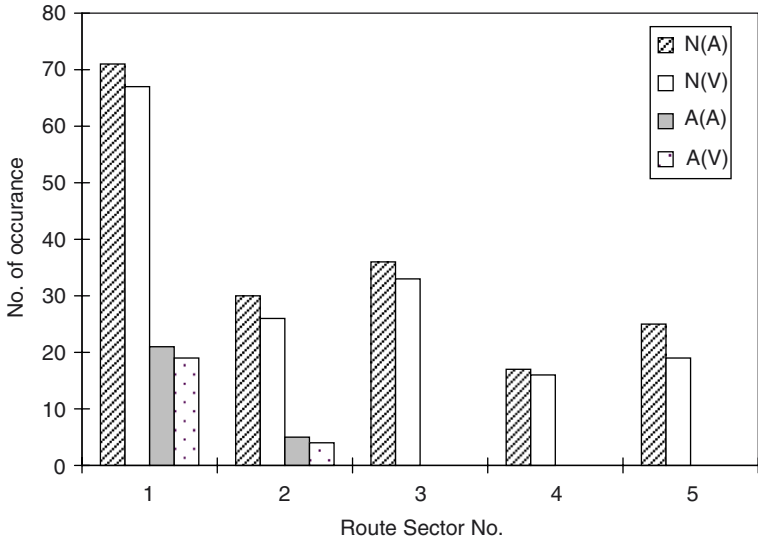

Fig. 7. A plot of frequency distribution patterns for air mass movement routes (all route types of 1–5) on the basis of back-trajectory analysis. For the full information of five different route sector numbers shown on x-axis, refer to Table 5. In legend box, symbols of N and A denote the period of non-Asian Dust (NAD) and Asian Dust (AD), respectively. In addition, letters of A and V in the parenthesis denote the number of all and valid cases, respectively.

notation defined as valid case in Fig. 7). The results of frequency analysis indicate that R1 case is the most abundant in all transport route types. It should however be noted that R1 cases can be further divided into two origin types with their extent of air pollution distinguished to each other. In a recent study of Sun et al. (2005), chemical composition of dust storms reaching in Beijing area was analyzed in relation to transport routes of AD. These authors have shown that a transport route with the north-northwesterly origin is less polluted, while the one for the westerly origin being more polluted. Consequently, our transport route of R1 were broken down into two sub-categories of R1A and R1B to represent northern and southern China, respectively (refer to Fig. 6). Note that the two contrasting routes of R1A and R1B in this study are comparable to the north-northwesterly and westerly origin defined by Sun et al. (2005). However, this subgrouping scheme was not meaningful for AD period, as all R1 cases in this study unanimously belonged to R1A only.

In an effort to decouple the effects of AD events from transport routes, Pb concentration data for all routes were evaluated statistically between AD and NAD period across three different particle fractions (Table 5). To help assess Pb distribution from such respect, the concentration data for both PM and the concurrently measured Al were also analyzed in the same manner. Comparison of these statistical parameters shown in Table 5 generally indicates that Pb concentrations tend to be smaller during AD than during NAD period, while those of PM and Al exhibit a reversed pattern. In order to make a meaningful comparison out of these results, all data for each transport route were evaluated by a normalization procedure in the next stage. To this end, the mean concentrations during NAD period were derived initially by pooling the average data sets of each component for all five routes measured in this study. As shown in Fig. 8, the concentration data for each route (Table 5) were then normalized by the NAD mean concentration values computed for each compound. The results of this comparison clearly indicate that Pb concentrations during AD period, represented only by two routes of R1 and R2, are much lower than those derived for NAD period. It is found that Pb concentration for R2 during AD is the lowest of all routes compared in this study. On the other hand, the highest Pb concentration is in fact found from R5 during NAD in which air masses were generally retained in the local area rather than being transported from distant sources. It is also interesting to find that Pb concentration in R5 (during NAD) is higher in coarse rather than fine fraction, while those of R1 and R2 during AD show a contrary pattern. Because all R1 cases during AD only represent less polluted air from R1A sector (than from R1B sector), the results seen in this comparison may be limited to explain such differences to a certain degree. However, the relative patterns for both PM and Al are quite different from those of Pb in that their concentrations are significantly lower during NAD than during AD period, regardless of transport routes. Like the patterns observed in this study, a previous study of LRTAP

Table 5
A statistical summary of three airborne pollutants (PM, Pb, and Al) measured during the entire study period

Route type[a]	Parameter	PM ($\mu g\,m^{-3}$)			Pb ($ng\,m^{-3}$)			Al ($ng\,m^{-3}$)		
		Fine	Coarse	PM10	Fine	Coarse	PM10	Fine	Coarse	PM10
R1(A)	Mean	75	172	242	84	44	115	2009	3378	5125
	SD	48	256	277	42	46	64	2562	2506	5105
	Median	66	78	124	79	27	127	1085	2274	3062
	Min	34	20	78	25	3	36	351	380	148
	Max	218	1006	1073	183	148	222	10,938	9841	20,778
	N	17	16	16	15	14	16	17	15	16
R2(A)	Mean	51	99	150	57	18	61	1149	3583	4732
	SD	24	40	62	39	17	25	947	1557	2472
	Median	52	103	150	44	18	74	1202	3839	5041
	Min	25	53	89	27	5	32	208	1594	1802
	Max	73	139	212	101	30	77	1985	5060	7045
	N	4	4	4	3	2	3	4	4	4
R1A(N)	Mean	73	44	116	103	45	129	255	992	1247
	SD	89	38	111	81	20	85	255	743	1050
	Median	46	28	75	89	48	99	160	799	930
	Min	13	11	41	24	8	26	28	124	67
	Max	479	185	587	317	88	327	963	2959	3864
	N	26	24	26	24	17	25	27	24	27
R1B(N)	Mean	92	27	69	97	65	130	203	676	841
	SD	189	19	27	62	55	79	206	564	721
	Median	46	24	62	90	45	111	134	610	555
	Min	27	3	35	24	8	50	35	34	113
	Max	846	76	120	221	193	283	807	2045	2408
	N	18	14	17	13	9	13	18	17	18
R2(N)	Mean	45	34	67	79	36	79	148	709	769
	SD	26	16	30	61	25	41	152	597	685
	Median	38	34	70	57	36	73	105	564	567
	Min	13	2	15	21	4	20	24	11	16
	Max	136	59	121	203	78	182	687	2153	2343
	N	19	16	20	14	8	18	19	18	21
R3(N)	Mean	29	41	63	75	40	121	143	426	510
	SD	18	82	81	54	33	93	139	379	480
	Median	23	26	49	58	28	90	100	339	416
	Min	6	5	6	30	6	34	14	42	48
	Max	75	420	446	248	97	347	531	1452	1934
	N	28	24	28	17	8	18	27	24	27
R4(N)	Mean	36	16	52	55	55	110	155	483	589
	SD	19	11	19	42	22	50	103	424	507
	Median	32	20	51	51	52	105	142	381	454
	Min	10	1	20	21	31	45	19	4	15
	Max	77	29	80	139	84	187	335	1074	1316
	N	9	9	9	7	4	5	10	9	10
R5(N)	Mean	88	35	84	108	87	157	269	721	928
	SD	54	16	34	77	85	84	192	515	634
	Median	72	34	91	75	64	171	240	648	827
	Min	38	4	8	26	9	38	38	114	58
	Max	230	53	147	245	253	296	776	1517	1831
	N	14	7	14	14	8	13	14	14	15

All results are compared between air mass movement routes and between particle fractions.

[a]Air mass movement routes to the study area based on back-trajectory analysis: Routes 1–5 are initially classified such as air mass passing from China (W), N. Korea (N), E. Sea (E), S. Sea (S), and local area (L), respectively. R1 type is divided further into R1A and R1B to represent air masses passing from north and south China, respectively. Letters of A and N in the parenthesis denote Asian Dust (AD) and Non-Asian Dust (NAD) period, respectively.

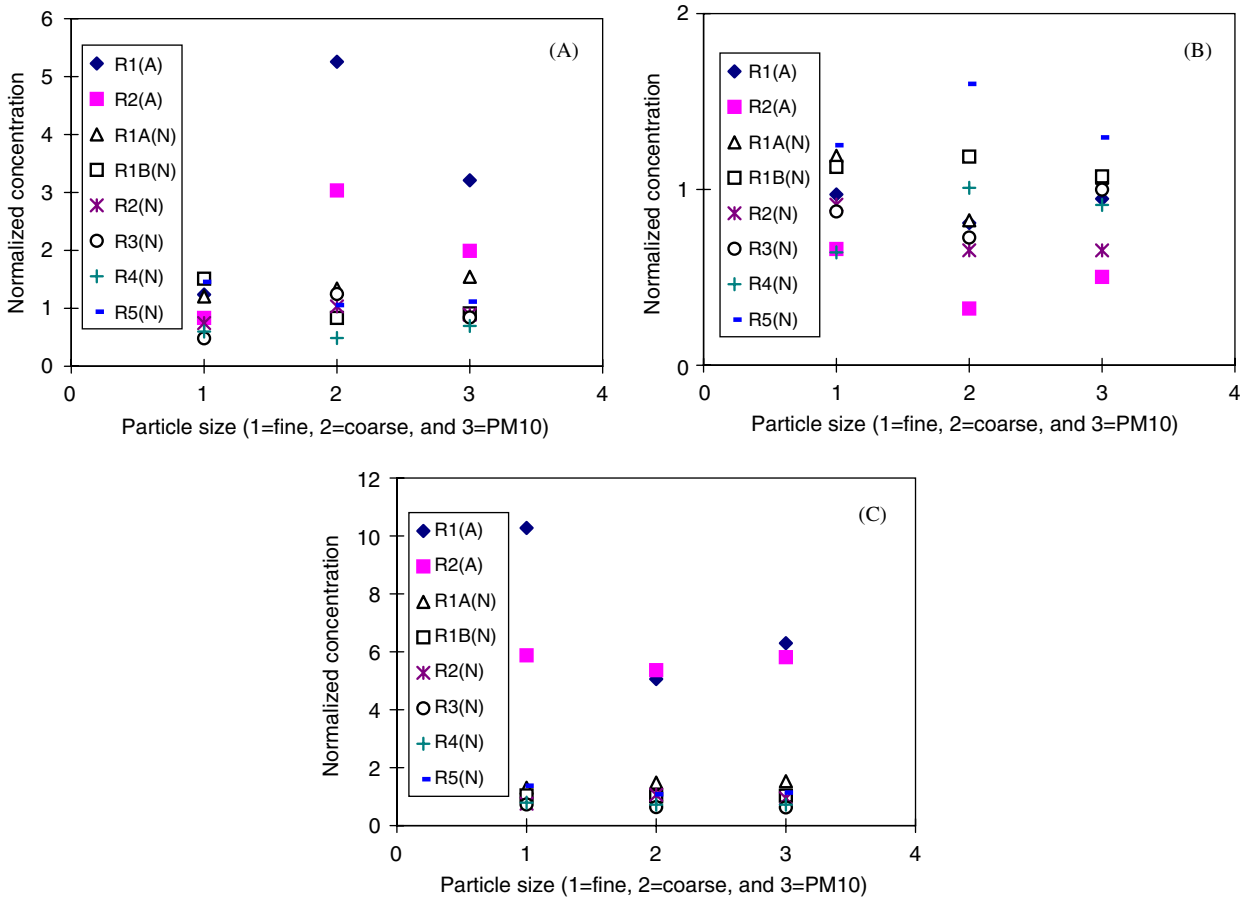

Fig. 8. The concentrations of three airborne pollutants ((A) PM, (B) Pb, and (C) Al) are compared between particle size fractions and between air mass movement routes. Letters of A and N in the parenthesis denote Asian Dust (AD) and Non-Asian Dust (NAD) period.

effect in the Hong Kong area also showed a pronounced increase in the relative abundance of elements of natural origin (e.g., Al, Fe, Ca, S, and Cl) in the episodic dust samples (Fang, Zheng, Wang, Chim, & Kot, 1999). The results of this comparative study based on trajectory analysis thus confirm that Pb concentrations in the study area can be affected more effectively by local, rather than distant, sources.

4. Conclusion

In this study, we investigated the influence of AD on the Pb distribution patterns using the springtime metal concentration data collected over four consecutive years. The results of our study indicate that the inflow of particles increase in all particle fractions during the AD (relative to the NAD period). Although such changes appear to be dominated by an increase in PM mass concentrations of the coarse fraction, those particles are generally deficient of some hazardous metallic components including Pb. Consequently, despite significant increases in coarse particle concentrations during the AD period, Pb concentrations can experience a moderate reduction due to a dilution induced by the abundance of Pb-depleted coarse particles. Such a mechanism may be important in affecting Pb concentration between the AD and NAD periods. However, there is also an opposing mechanism in which Pb-enriched fine particles can be introduced as the result of the AD events during a certain period. Hence, when our measurement data are examined in terms of their relationship with the AD event, we may have to acknowledge the possibility of the two contrasting mechanisms at work. First of all, as seen in the year 2002, the dilution effect caused by the intrusion of metal-depleted, coarse particles can lead to a reduction of the Pb concentration levels. However, as it was the case for 2001, the Pb concentration levels

during the AD period can exceed those during the NAD period due to the preferential enrichment of Pb in the fine fraction.

In order to account for Pb concentration levels in relation to such variables as the occurrences of AD and air mass transport pathways, all of our Pb data were compared and evaluated after being grouped into such criteria. The results of this comparative analysis indicate that the distribution of Pb can be clearly distinguished from those of PM or other particle-bound pollutants. When all measurement data collected for the four year time span are compared between AD and NAD period, Pb concentrations in the study area can decrease considerably during AD period; however, it seems to peak during NAD, especially when air masses are retained in the local area. The pattern of Pb between AD and NAD period thus sharply contrasts with those of PM or other metals (such as Al) which tend to exhibit significantly increased concentration levels with the inflow of AD storms from westerly sources. It is thus suggested that the occurrences of AD events, while having a potential to increase the concentrations of some pollutants, can also facilitate the reduction of others in which Pb-enriched local dusts are mixed with Pb-depleted dusts from long distant sources.

Acknowledgements

This research was carried out with a financial support of the Korea Polar Research Institute, KORDI (Grant PP06010). The authors are grateful to the constructive criticism provided by two anonymous reviewers. The authors would also like to thank NOAA/ARL for providing HYSPLIT model and meteorological data.

References

Arndt, R. L., Carmichael, G. R., Streets, D. G., & Bhatti, N. (1997). Sulfur dioxide emissions and sectorial contributions to sulfur deposition in Asia. *Atmospheric Environment*, *31*, 1553–1572.

Carmichael, G. R., Hong, M. S., Ueda, H., Chen, L. L., Murano, K., Park, J. K. et al. (1997). Aerosol composition at Cheju Island, Korea. *Journal of Geophysical Research*, *102*(5), 6047–6061.

Chun, Y. S., Kim, J. Y., Choi, J. C., Boo, K. O., Oh, S. N., & Lee, M. H. (2001). Characteristic number size distribution of aerosol during Asian dust period in Korea. *Atmospheric Environment*, *35*, 2715–2721.

Chung, Y. S., & Yoon, M. B. (1996). On the occurrence of Yellow Sand and atmospheric loading. *Atmospheric Environment*, *30*(13), 2387–2397.

Draxler, R. R. (1996). Boundary layer isentropic and kinematic trajectories during the August 1993 North Atlantic Regional Experiment Intensive. *Journal of Geophysical Research*, *101*(D22), 29255–29268.

Draxler, R. R. (2001). *Hybrid single-particle Lagrangian integrated trajectories* (*HYSPLIT*): *Version* 4.5. User's Guide and Model Description. NOAA Technical Memorandum ERL ARL-230, 35pp.

Fang, G. C., Chang, C. N., Wu, Y. S., Fu, P. P. C., Yang, C. J., Chen, C. D. et al. (2002). Ambient suspended particulate matters and related chemical species study in central Taiwan, Taichung during 1998–2001. *Atmospheric Environment*, *36*, 1921–1928.

Fang, M., Zheng, M., Wang, F., Chim, K. S., & Kot, S. C. (1999). The long-range transport of aerosols from northern China to Hong Kong—a multi-technique study. *Atmospheric Environment*, *33*, 1803–1817.

Ho, K. F., Lee, S. C., Chan, C. K., Yu, J. C., Chow, J. C., & Yao, X. H. (2003). Characterization of chemical species in PM2.5 and PM10 aerosol in Hong Kong. *Atmospheric Environment*, *37*, 31–39.

Kai, K., Okada, Y., Uchino, O., Tabata, I., Nakamura, H., Takasugi, T. et al. (1988). Lidar observation and numerical simulation of a Kosa (Asian dust) over Tsukuba, Japan during the Spring of 1986. *Journal of Meteorological Society of Japan*, *66*, 457–472.

Kanamitsu, M. (1989). Description of the NMC global data assimilation and forecast system. *Weather and Forecasting*, *4*, 335–342.

Kim, K.-H., Choi, B. J., Yun, S. T., & Hwang, S. J. (2004). Studies of spatial and temporal distribution characteristics of TSP-bound trace metals in Seoul, Korea. *Environmental Pollution*, *127*(3), 323–333.

Kim, K.-H., Choi, G.-H., Kang, C. H., Lee, J.-H., Kim, J. Y., Youn, Y. H. et al. (2003). The chemical composition of fine and coarse particles in relation with the Asian Dust events. *Atmospheric Environment*, *37*(6), 753–765.

Kim, K.-H., Kim, D. S., & Lee, T. J. (1997). The temporal variabilities in the concentrations of airborne lead and its relationship to aerosol behavior. *Atmospheric Environment*, *31*(20), 3449–3458.

Kim, K.-H., & Kim, M. Y. (2003). The effects of Asian Dust on particulate matter fractionation in Seoul, Korea during spring 2001. *Chemosphere*, *51*(8), 707–721.

Kim, K.-H., Lee, J.-H., & Jang, M. S. (2002). Metals in airborne particulate matter from the first and second industrial complex area of Taejon city, Korea. *Environmental Pollution*, *118*, 41–51.

Kim, K.-H., & Song, D. W. (1997). The concentrations of lead in urban and nonurban atmospheres of Won Ju city, Korea. *Water, Air and Soil Pollution*, *98*(3–4), 225–273.

Lin, T. H. (2001). Long-range transport of yellow sand to Taiwan in spring 2000: Observed evidence and simulation. *Atmospheric Environment*, *35*, 5873–5882.

McKendry, I. G., Hacker, J. P., Stull, R., Sakiyama, S., Mignacca, D., & Reid, K. (2001). Long-range transport of Asian dust to the Lower Fraser Valley, British Columbia, Canada. *Journal of Geophysical Research*, *106*(D16), 18361–18370.

Mishra, V. K., Kim, K.-H., Kang, C.-H., & Choi, K. C. (2004). Wintertime sources and distribution of airborne lead in Korea. *Atmospheric Environment*, *38*, 2653–2664.

Perry, K. D., Cahill, T. A., Schnell, R. C., & Cahill, J. M. (1999). Long-range transport of anthropogenic aerosols to the National Oceanic and Atmospheric administration baseline station at Mauna Loa Observatory, Hawaii. *Journal of Geophysical Research*, *104*(D15), 18521–18533.

Streets, D. G., Tsai, N. Y., Akimoto, H., & Oka, K. (2000). Sulfur dioxide emissions in Asia in the period 1985–1997. *Atmospheric Environment*, *34*, 4413–4424.

Sun, Y., Zhuang, G., Wang, Y., Zhao, X., Li, J., Wang, Z. et al. (2005). Chemical composition of dust storms in Beijing and implications for the mixing of mineral aerosol with pollution aerosol on the pathway. *Journal of Geophysical Research*, *110*, D24209.

Zhang, X., & Arimoto, R. (1993). Atmospheric trace elements over source regions for Chinese dust: Concentrations, sources and atmospheric deposition on the losses plateau. *Atmospheric Environment*, *27A*(13), 2051–2067.